Improving the Electrocatalytic Activities and CO Tolerance of Pt NPs by Incorporating TiO_2 Nanocubes onto Carbon Supports

Rodolfo M. Antoniassi,[a] Jhon Quiroz,[a, b] Eduardo C. M. Barbosa,[a] Luanna S. Parreira,[a] Roberta A. Isidoro,[c] Estevam V. Spinacé,[c] Julio C. M. Silva,[d] and Pedro. H. C. Camargo*[a, b]

Designing efficient anode CO-tolerant electrocatalysts is critical in low-temperature fuel cell catalysts fueled either by H_2/CO or alcohol. We demonstrate that the incorporation of TiO_2 nanocubes (TiO_2NCs) on Carbon Vulcan supports, followed by the synthesis of Pt NPs at their surface (Pt/TiO_2NCs-C material), led to improvements in performance towards the electrooxidation of carbon monoxide, ethanol, methanol, ethylene glycol, and glycerol in acidic media relative to the commercial Pt/C and Pt/TiO_2-C counterparts employing commercial TiO_2. The nanocubes enabled changes in the electronic properties of Pt NPs while contributing to the bifunctional mechanism as compared to Pt/C and Pt/TiO_2-C with commercial TiO_2. Fuel cell experiments fed with H_2/CO steam showed that Pt/TiO_2NCs-C employing nanocubes was resistant to CO-poisoning, yielding superior performance in operational conditions. The results reported herein have important implications for developing electrocatalysts with superior performances in PEMFCs.

Introduction

Direct Alcohol Fuel Cells (DAFC) have emerged as a promising alternative device to the H_2-fueled Proton Exchange Membrane Fuel Cell (PEMFC) for power generation in portable applications.[1,2] The electrooxidation of short-chained organic molecules, such as alcohols, have been extensively studied over the past decades.[3–8] These molecules represent a viable option relative to the use of pure H_2 from the expensive process of water electrolysis.[9] Among all types of alcohol, ethanol presents important advantages as compared to H_2 and other low-molecular alcohols. These including cheap large-scale production from biomass, non-toxicity, easy storage in liquid tanks at ambient temperature, and high molecular energy density.[3,10,11] Nevertheless, finding efficient catalysts, which can balance the performance, selectivity, and stability tripod is the main drawback for the commercialization of both DAFCs and the so-called CO-contaminated H_2 (H_2/CO-fed PEMFCs).

Carbon supported platinum nanoparticles (Pt NPs) are the most active materials for both anode and cathode electrodes in PEMFC or DAFCs devices.[12–14] However, incomplete alcohol fragments such as CO and CH_3-species strongly adsorb onto the Pt surface slowing down the kinetics due to poisoning effects.[15,16] Specifically, CO strongly hinders the Pt active sites and limits the catalytic turnover,[17] thereby reducing the overall efficiency of practical systems supplied with alcohol or H_2/CO steam by causing overpotential losses.[10] It is worth mentioning that the CO-poisoning of Pt-based catalysts in fuel cell devices is a common effect faced by either alcohol or contaminated H_2 produced by hydrocarbons steam reforming processes. Therefore, the development of more active and CO-tolerant catalysts in oxidizing alcohols and H_2/CO steam represents an important challenge. In this context, many studies have focused on combining Pt with other CO-resistant elements like Ru, Sn, Cu, and Ni (generating bimetallic NPs) and on the control over the NPs shape in supported Pt and Pt-based nanomaterials.[16,18–26]

In addition to electrocatalytic activity, the stability of PEMFC electrodes is a significant hurdle to their application as vehicular and stationary/portable suppliers, especially when such devices are operated upon the cyclic regime. The deterioration of Pt/C-based catalysts results either from the reduction in the number of Pt active sites (due to leaching and/or agglomeration) or the corrosion of carbon support.[27–31] For example, Pt NPs aggrega-

[a] Dr. R. M. Antoniassi, Dr. J. Quiroz, Dr. E. C. M. Barbosa, Dr. L. S. Parreira, Prof. P. H. C. Camargo
Instituto de Química (IQ)
Universidade de São Paulo (USP)
Cidade Universitária
Av. Prof. Lineu Prestes, 748
São Paulo, SP 05508-000 (Brazil)
[b] Dr. J. Quiroz, Prof. P. H. C. Camargo
Department of Chemistry
University of Helsinki
A.I. Virtasen aukio 1
Helsinki (Finland)
E-mail: pedro.camargo@helsinki.fi
[c] Dr. R. A. Isidoro, Dr. E. V. Spinacé
Instituto de Pesquisas Energéticas e Nucleares
IPEN/CNEN-SP
Cidade Universitária
Av. Prof. Lineu Prestes, 2242
São Paulo, SP 05508-900 (Brazil)
[d] Prof. J. C. M. Silva
Instituto de Química da Universidade Federal Fluminense
Grupo de Eletroquímica e Materiais Nanoestruturados
Campus Valonguinho
Niterói, RJ 24020-141 (Brazil)

Supporting information for this article is available on the WWW under https://doi.org/10.1002/cctc.202002066

tion originated from the dissolution/re-deposition of the Pt, and the motion of the Pt atoms onto the carbon surface is regarded as the main reason for the reduction of the catalyst activity.[29] Meanwhile, the electrochemical mechanism of the support corrosion in acid fuel cells shows that carbon electrolyzes water in the presence of Pt to yield CO and CO_2 as products.[32]

The optimization of metal-support interactions represents a promising strategy to tackle and enhance the stability of Pt NPs in electrocatalytic applications.[33] This has been pursued, for example, by synthesizing shape-controlled carbon surfaces such as sheets, tubes, and horns,[34] by doping carbon with heteroatoms,[35–37] and by the addition of metal oxides in the carbon supports, including TiO_2, CeO_2, WO_3.[38–41] Interestingly, metal oxides can also act as sources of oxygen, which is involved in promoting the carbon monoxide removal from the Pt NPs surface during the electrooxidation reactions as well as promoting changes in the metal-support interactions. Inspired by these guidelines, we report on the effect of the control over the shape of the metal oxide added to the carbon support in Pt-based electrocatalytic materials. Precisely, we targeted the addition of TiO_2 nanocubes (TiO_2NCs) onto carbon and employed the resulting material as hybrid support for the deposition of Pt NPs, which was subsequently evaluated as an electrocatalyst towards carbon monoxide, methanol, ethanol, ethylene glycol, glycerol, and CO-contaminated H_2 electrooxidation. Surprisingly, we found that the use of TiO_2NCs in the support enables higher electrocatalytic activities and stability as compared to the conventional Pt/C material and the Pt/TiO_2-C electrocatalyst counterpart prepared by using commercial TiO_2 NPs.

Experimental

The following materials were used as received: analytical grade hexachloroplatinic (IV) acid hexahydrated ($H_2PtCl_6 \cdot 6H_2O$, 99.9%, Sigma-Aldrich) as metal precursor, Carbon Vulcan (XC72R, 99%, Cabot Corporation), DI water (18.2 MΩcm), H_2SO_4 (sulfuric acid PA, Casa Americana), Nafion solution 5 wt.%, Sigma-Aldrich, Nafion membrane 115 (Dupont), C_3H_7O (anhydrous isopropyl alcohol, 99.5%, Sigma-Aldrich), CH_4O (absolute methanol, Sigma-Aldrich), $C_2H_6O_2$ (absolute ethanol, Sigma-Aldrich), $C_2H_6O_2$ (ethylene glycol, 99.5%, Vetec) and $C_3H_8O_3$ (glycerol, 99%, Sigma-Aldrich), $C_2H_4O_2$ (acetic acid, 99.7%, Synth), $C_6H_8O_6$ (ascorbic acid, 99%, BioXtra), 1-butyl-3-methylimidazolium tetrafluoroborate ([bmin][BF_4], 97%, Sigma-Aldrich), titanium tetrabutoxide ($Ti(OBu)_4$, 97%, Sigma-Aldrich), commercial TiO_2 (titanium (IV) oxide, 99%, Sigma-Aldrich), Pt/C and PtSn/C (both 20% metal load, purchased from Etek (lot# F03081022 and F0930209, respectively).

Synthesis of TiO_2NCs

The TiO_2 nanocubes were synthesized using a modified hydrothermal procedure.[42] Typically, a mixture containing 1 mL of [bmin][BF_4], 40 mL of acetic acid, and 2.5 mL of DI water was stirred in a beaker. After 10 minutes, 5 mL of $Ti(OBu)_4$ were added dropwise to the reaction mixture. This system was kept under stirring for 30 minutes. After 5 minutes of ultrasonic treatment, the mixture was put in a 220 mL Teflon-lined autoclave and heated up to 180 °C. After 18 hours, the autoclave was allowed to cool to room temperature under ambient conditions. The solid product was isolated from the reaction mixture and washed with water and ethanol by successive rounds of centrifugation (5 minutes at 6500 rpm), removal of the supernatant, and re-dispersion. The TiO_2NCs were then dried under a high vacuum at room temperature.[42]

Synthesis of Pt NPs supported on TiO_2NCs-C (Pt/TiO_2NCs-C) and Pt/TiO_2-C employing ethylene glycol (EG) reducing agent

Here, three kinds of supports were evaluated: Pt NPs supported on Vulcan Carbon (from commercial Pt/C, Etek); Pt NPs supported on TiO_2 nanocubes and C (Pt/TiO_2NCs-C); and Pt NPs supported on commercial TiO_2 and C (Pt/TiO_2-C). Pt NPs supported on TiO_2NCs-C and TiO_2-C materials were prepared by a modified alcohol reduction method.[43] In a typical synthesis, a suspension containing EG/H_2O (3:1 volume), TiO_2, and C supports (corresponding to 80 wt.%) was sonicated for 10 min. The prepared suspensions were heated at 150 °C under vigorous stirring. After the temperature was reached, 2.12 mL of $H_2PtCl_6 \cdot 6H_2O$ solution (0.05 g mL^{-1}) was quickly added, and the resulting mixtures were kept under reflux for another 3 h. The nominal Pt loading was fixed in 20 wt.% in both materials. The products were isolated from the reaction mixture and washed with water by successive rounds of centrifugation, removal of the supernatant, and re-dispersion. Finally, the produced electrocatalysts were dried at 80 °C for 2 h (Scheme S1, Supporting Information). The content of cubic TiO_2NCs was varied from 5 to 40 wt.% and different Carbon amounts were employed (75–40 wt.%) to keep the platinum load in 20%. For Pt/TiO_2-C commercial preparation, it was chosen 10% of TiO_2 and 70% of Vulcan Carbon.

Characterization

The size and morphology of the prepared materials were characterized by Scanning Electron Microscopy (SEM, using a JEOL JSM 6330F operating at 5 kV) and Transmission Electron Microscopy (TEM, JEOL JEM 2100F operated at 200 kV). SEM sample was prepared by drop-casting an aqueous suspension of TiO_2NCs material onto a silicon wafer, followed by drying at ambient temperature. For TEM analysis, a small amount of the catalyst was suspended in isopropyl alcohol and dropped in a TEM copper grid coated with colloidal film. Size was measured by end-to-end of particle extension. Composition analysis was conducted by X-ray dispersive spectroscopy (EDS), coupled to an SEM microscope JEOL JSN 6010LA, operated at 20 kV. X-ray diffraction analyses were performed using a Bruker D2 Phaser equipment with a Cu Kα source. The integration time was set to 1 minute using 0.05° step, ranging from 20° to 90°. The sample was placed on an acrylic holder and the slit used measured 1.0 mm.

X-ray photoelectron spectra (XPS) were taken with a Thermo Scientific K-Alpha spectrometer using a 72 W monochromated Al K alpha source ($h\nu = 1486.6$ eV. The pass energy was set to 40 eV, with 0.1 eV step and 1 s per point of acquisition time. The sample holders were transferred to the XPS pre-chamber in an inert atmosphere and held under a vacuum. All XPS were referenced according to the adventitious C 1s peak (285 eV). All binding energies were referenced to the C 1s core level at 285 eV. Simulation of the experimental photopeaks was carried out using a mixed Gaussian/Lorentzian peak fit procedure according to the software supplied by CasaXPS. The semiquantitative analysis accounted for a nonlinear Shirley background subtraction.

Electrochemical measurements

All the electrochemical measurements were performed by 910 PSTAT (Metrohm) potentiostat. A three-electrodes cell apparatus with an ultrathin vitreous carbon layer previously polished was used as a working electrode (WE). For the WE preparation, a sonicated aliquot (5 μL) of a catalytic dispersion containing 0.9 mL of water, 0.1 mL of isopropyl alcohol, 20 μL of Nafion solution and was dropped in the tip of the vitreous carbon layer and dried (totalizing about 2 μg of Pt on the WE). Sulfuric acid (0.5 mol L^{-1}) was employed as a supporting electrolyte. Cyclic voltammograms (CV) were recorded after N_2 gas was bubbled for 30 min into the electrolyte. CV recordings had a scan rate of 0.05 V s^{-1} at ambient temperature. Cyclic voltammetry experiments of methanol, ethanol, ethylene glycol and glycerol electro-oxidation reactions were conducted in 1 mol L^{-1}. For the CO-stripping experiment, the WE was submitted to 0.35 V polarization and carbon monoxide was bubbled for 500 s into the electrolyte, followed by 800 s of N_2. For further comparison purposes, the electroactive area (ECSA) was calculated based on the hydrogen desorption profile through the voltammetry of the CO-stripping experiment data by Equation [1].

$$ECSA = \frac{Q_H}{[Pt]q^0_H} \quad (1)$$

where Q_H is the hydrogen desorption charge from 0.05–0.4 V, considering the electrical double layer contribution; *[Pt]* is the platinum loading and q^0_H is the charge required to oxidize a hydrogen monolayer adsorbed over platinum (210 μC cm^{-2}).

Fuel Cell performance

For Membrane Electrode Assembly (MEA) preparation, Pt/C and Pt/TiO_2NCs-C were evaluated as anode and Pt/C as the cathode, both electrodes loaded with 0.6 mg_{Pt} cm^{-2}. The 5 cm^2 electrodes were hot-pressed to a pre-treated Nafion 115 membrane (Dupont) at 125 °C for 10 min. All prepared MEAs were inserted in a single cell, operating at 80 °C, fueled with H_2 and H_2/CO gases (100 ppm CO – 300 mL min^{-1}) on the anodic side and O_2 supplying the cathodic side (200 mL min^{-1}). No pressure was used in the cathode. Polarization curves were employed to evaluate the catalyst's electrical performance.

Results and discussion

Figure 1a depicts the SEM images for the TiO_2NCs that were employed as substrates for the deposition of Pt at their surface. It can be observed that the TiO_2 nanocubes are well defined, relatively monodisperse, and their edge lengths corresponded to 72 ± 9 nm. The nanocubes were then mixed with carbon (20 mg of TiO_2NCs and 140 mg of C) to generate our support material (TiO_2NCs-C), which was employed as physical templates for the deposition of Pt at their surface. Figure 1b and Figure 1c show HRTEM images for the Pt/TiO_2NCs-C material obtained after Pt deposition. The 0.36 nm lattice spacings characteristic of TiO_2 anatase can be detected, corresponding to the growth along the (100) crystallographic direction and the exposure of (100) surface facets in agreement with the nano-

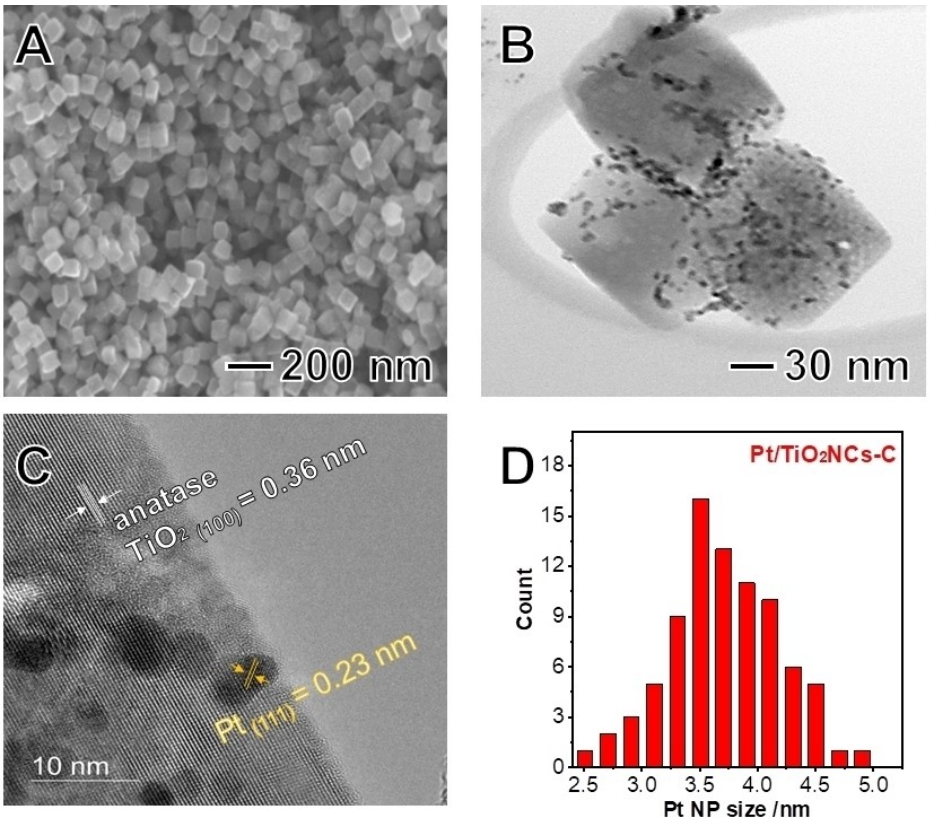

Figure 1. (A) SEM image of TiO_2NCs. (B and C) HRTEM image of the Pt/TiO_2NCs-C materials. (D) Histogram of the size distribution for the Pt NPs of Pt/TiO_2NCs-C.

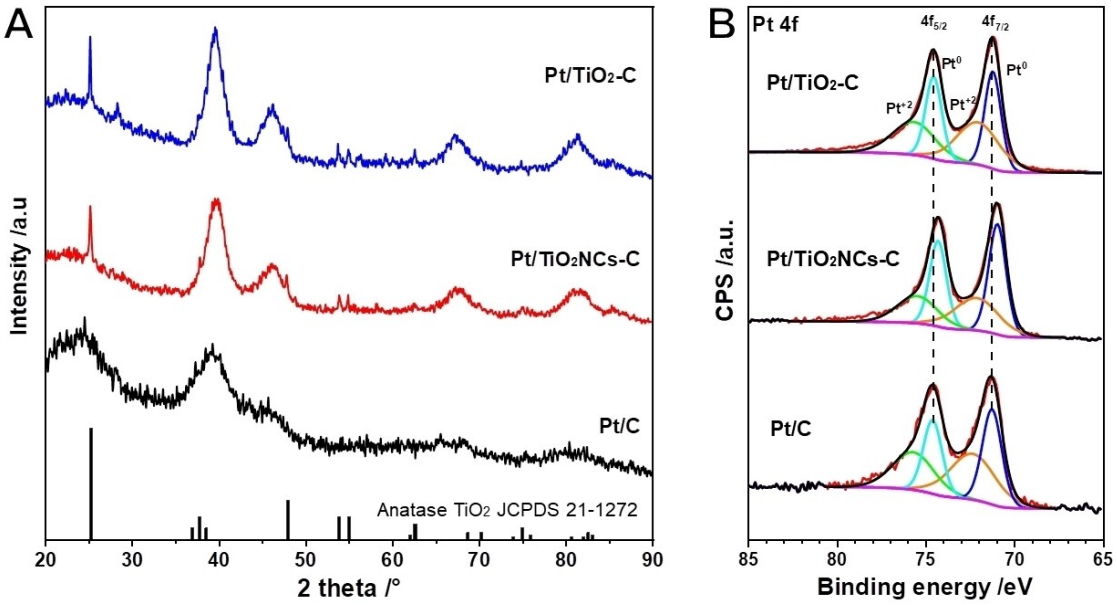

Figure 2. XRD patterns (A) and XPS Pt 4f core-level spectra (B) for Pt/C (bottom trace), Pt/TiO_2NCs-C (middle trace), and Pt/TiO_2-C (top trace).

cube morphology.[44] It can also be observed that the Pt NPs were deposited at the surface of the TiO_2 nanocubes had a spherical shape and narrow particle size distribution. The histogram of the particle size distribution (Figure 1d) indicated that the Pt NPs size corresponded to 3.7 ± 0.5 nm. The EDS spectra revealed that the Pt content corresponded to 20 wt.%, in agreement with the nominal Pt loading (Figure S1 and Table S1). The presence of Vulcan Carbon at the surface of the TiO_2NCs and Pt nanoparticles can be observed from Figure S3.

We also prepared similar Pt/TiO_2-C materials in which commercial TiO_2, instead of nanocubes, was employed to generate the TiO_2-C support and therefore served as a reference to evaluate the importance of the TiO_2 shape control over the synthesis and performance of the produced electrocatalysts. HRTEM images for the Pt/C and Pt/TiO_2-C materials in which commercial TiO_2 (instead of nanocubes) was employed as reference support are shown in Figure S2a and S2b, respectively. For Pt/C, the Pt NPs were spherical and uniformly dispersed over the support. Their diameter corresponded to 3.2 ± 0.5 nm (Figure S2c). For Pt/TiO_2-C material in which commercial TiO_2 was employed as support, Pt NPs 4.0 ± 0.6 nm in size were obtained (Figure S2d). However, they were not uniformly dispersed at the surface of the TiO_2, and significant agglomeration could be detected. Therefore, our data indicate that the utilization of TiO_2NCs was essential to achieve better dispersion of Pt NPs at the TiO_2 surface (relative to the commercial counterpart).

Figure 2a shows the XRD patterns of Pt/TiO_2NCs-C, Pt/TiO_2-C, and Pt/C. The diffractograms show characteristic peaks for *fcc* Pt in all cases at 2theta = 39°, 46°, 67°, 81°, 86°. A broad peak in 25° can be assigned to the presence of amorphous carbon, while characteristic peaks assigned to the anatase structure of TiO_2 (JCPDS, no. 21-1272) could be detected in the materials containing TiO_2. The Pt crystallite size estimated by Scherrer equation (using the peak at 2theta = 39°) corresponded to about 4 nm, in agreement with the HRTEM results.

Figure 2b depicts the Pt 4f core-level XPS for the Pt/TiO_2NCs-C, Pt/TiO_2-C, and the Pt/C (top to bottom traces, respectively). The binding energy (BE) values, full width at half maximum, and Pt surface percentages are given in Table 1. For

Table 1. Pt surface species assignment, binding energy, FWHM, and surface percentage values calculated from XPS analysis (Figure 2B).

Sample	Pt Species	Binding Energy [eV]	FWHM [eV]	Percentage [%]
Pt/C	$Pt^0_{7/2}$	71.2	1.3	26.8
	$Pt^{2+}_{7/2}$	72.3	3.0	30.4
	$Pt^0_{5/2}$	74.6	1.2	20.0
	$Pt^{2+}_{5/2}$	75.7	2.8	22.8
Pt/ TiO_2NCs-C	$Pt^0_{7/2}$	70.9	1.1	32.6
	$Pt^{2+}_{7/2}$	72.1	2.9	24.6
	$Pt^0_{5/2}$	74.3	1.1	24.4
	$Pt^{2+}_{5/2}$	75.4	2.6	18.4
Pt/TiO_2-C	$Pt^0_{7/2}$	71.2	1.1	25.7
	$Pt^{2+}_{7/2}$	72.0	2.8	29.7
	$Pt^0_{5/2}$	74.5	1.1	21.6
	$Pt^{2+}_{5/2}$	75.6	2.8	23.0

all samples, the Pt 4f region showed two photoelectron peaks ascribed to Pt $4f_{7/2}$ and Pt $4f_{5/2}$ core-levels with BE values at around 70 and 74 eV. The Pt 4f region has been deconvoluted into two pairs of doublets, which can be attributed to Pt^0 and Pt^{II} species. It can be observed that for Pt/C and Pt/TiO_2-C catalysts the BE of Pt $4f_{7/2}$ of Pt^0 is located at 71.2 eV, while for Pt/TiO_2NCs-C this peak is at 70.9 eV. The decrease of the BE indicated that electrons can be transferred from TiO_2 nanocubes to Pt, resulting in a Pt surface with a more reduced state. This shift towards lower BE has already been reported for Pt supported on other TiO_2/C hybrid systems, suggesting that the electronic structure of Pt atoms can be modified by the TiO_2NCs as a result of strong metal-support interactions.[38,45,46] It has been reported that the interfacial effect between Pt and TiO_2 is dependent on the nature of the TiO_2 surface facets, in which (100) surface facets have been found to provide stronger charge transfer values in Pt/TiO_2 electrocatalysts having controlled shapes.[47] In this case, it is plausible that the TiO_2NCs present a larger fraction of (100) surface facets relative to the commercial TiO_2 NPs. Therefore, this increased fraction of (100) surface facets enables a higher charge transfer from TiO_2 to Pt NPs and thus stronger metal-support interactions relative to the commercial NPs.

To gain insights on the oxidation states of the Pt species over the surface of the catalysts, we examined the full width at half maximum and the atomic percentages of each Pt surface species obtained from the XPS data. The full width at half maximum values is higher for the Pt/C sample suggesting that more oxidized Pt (II) species are present on the surface of this material contributing to 53% of the registered signal. Interestingly, it can be detected that the Pt/TiO_2NCs-C sample displayed the highest percentage of Pt^0 relative to Pt^{II} as compared to the other samples. The Pt^0 content in this sample was increased by approximately 22% as compared to the Pt/C. These observations agree with an increased electron density at Pt as a result of enhanced metal-support interactions with the TiO_2 nanocubes in the support.[45,46] It is important to note that the precise estimation of the percentage of Pt loaded on TiO2 and C is challenging. Therefore, in our study, we made the approximation that Pt NPs are deposited over both TiO_2 and C during the synthesis procedure without any preferential deposition of one of the supports.

Figure 3 displays the CO-stripping profile for the electrooxidation features of a one-absorbed carbon monoxide layer on Pt/TiO_2-C (blue trace), Pt/TiO_2NCs-C (red trace), and the Pt/C (black trace). It is established that Pt has a structural-sensitive interaction with carbon monoxide, thus this molecule has been employed as a molecular probe to study the properties of Pt catalytic surfaces.[48] As can be observed from Figure 3, the CO-stripping features were different and thus sensitive to the nature of the Pt-based catalysts, indicating the presence and shape of TiO_2 support influenced the Pt surface properties. In the voltammetry curves for Pt/TiO_2NCs-C and Pt/TiO_2-C, the main CO electrooxidation peaks were negatively-shifted (ca. 0.86 V vs RHE) relative to Pt/C (bottom trace, 0.88 V vs RHE).[49] This indicates that the CO removal from the Pt surface is facilitated in the materials containing TiO_2. Moreover, differently

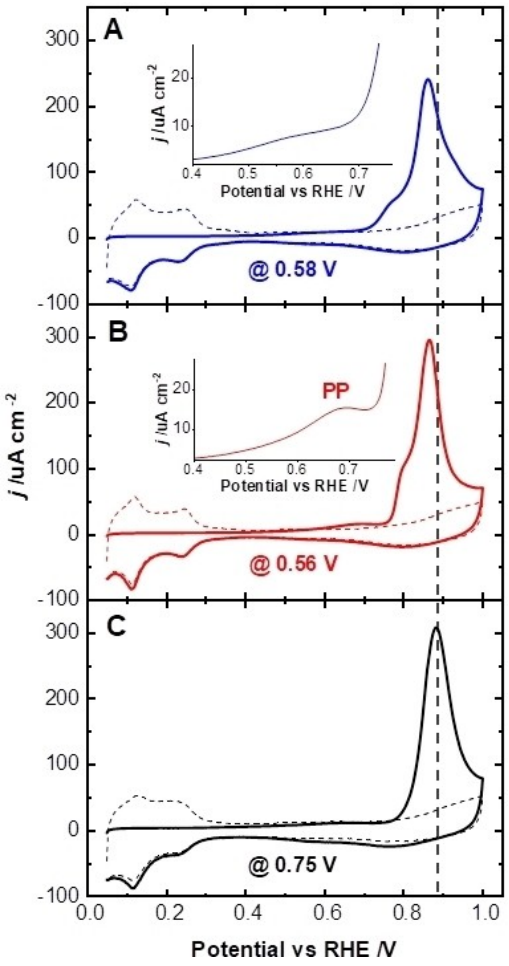

Figure 3. CO-stripping experiments recorded at 50 mV s^{-1} in 0.5 mol L^{-1} of H_2SO_4 at 25 °C. Carbon monoxide was adsorbed at 0.35 V vs RHE for 500 s before 800 s of N_2 purging. (A) Pt/TiO_2-C, B) Pt/TiO_2NCs-C and C) Pt/C. Graph insets of the Pre-peak (PP) indicated in the corresponding anodic scan region of the CO-stripping curves.

from Pt/C, both TiO_2-based materials exhibited a split-peak profile. Particularly, the CO-stripping voltammograms revealed the lower onset potential for Pt/TiO_2NCs-C (0.56 V vs RHE) and Pt/TiO_2-C (0.58 V vs RHE) relative to Pt/C (0.75 V vs RHE). Interestingly, for Pt/TiO_2NCs-C, the CO-stripping profile showed a visible pre-peak (highlighted in the inset) centered at ca. 0.68 V vs RHE, which could be a result of the strong metal-support interaction between the Pt NPs and the TiO_2 nanocubes (this pre-peak was not observed for the samples containing commercial TiO_2, the same region is highlighted as in the corresponding inset). This strong metal-support interaction contributes to the weakening of the Pt-CO interaction.[50–52] The calculated electroactive surface areas (ECSA) after the CO-stripping voltammograms corresponded to 72, 64, and 76 $m^2 g_{Pt}^{-1}$ for the Pt/TiO_2NCs-C, Pt/TiO_2-C, and Pt/C, respectively, indicating the values were relatively close for all catalysts in agreement with the similar Pt NPs sizes in the samples.

To reveal the influence of TiO_2NCs loading on the performance of the catalyst towards ethanol electrooxidation reaction

(EOR), we synthesized Pt/TiO_2NCs-C with different TiO_2NCs loadings. Figure S4 shows the maximum current density obtained from the forward scan in the corresponding CVs for Pt/TiO_2NCs-C as a function of the TiO_2NCs loading. Here, the Pt loading was maintained at 20 wt.% in all materials, while the composition of the support was varied. It can be observed that a volcano type relationship between maximum current density and TiO_2NCs loading was observed, with the peak in current density centered at 10 wt.% in mass of TiO_2NCs. Therefore, the TiO_2NCs loading was kept at 10 wt.% for all subsequent studies. The decrease in the current density values at higher TiO_2NCs loadings may be assigned to the decrease in the conductivity of the support. It can also be observed that the maximum current density for the Pt/TiO_2NCs-C (10 wt.% TiO_2NCs loading) was higher relative to the Pt/TiO_2-C sample (408 vs. 353 A g_{Pt}^{-1}). Such a difference in catalytical performance demonstrates that the proper choice of support morphology can lead to an improvement in the DAFC activity.[8]

We then focused on the investigation of the electrocatalytic activity of the Pt/TiO_2NCs-C and the state-of-art Pt/C towards the EOR. The EOR activity was evaluated by cyclic voltammetry, recorded in 0.5 mol L^{-1} of H_2SO_4 electrolyte containing 1 mol L^{-1} of ethanol. It can be observed from Figure 4a that Pt/TiO_2NCs-C showed higher activity than Pt/C. The maximum current density of the forward scan was 640 and 475 μA cm^{-2} for Pt/TiO_2NCs-C and Pt/C, respectively. Moreover, the onset potential (seen in the inset) for Pt/TiO_2NCs-C was lower than on the Pt/C material (0.41 vs 0.49 V, respectively), demonstrating the promotion effect of TiO_2NCs on the EOR. Figure 4b exhibits the maximum current density of the forward scan normalized by Pt mass (top panel) and specific area (bottom panel). It can be observed that the maximum current density by Pt load on Pt/TiO_2NCs -C was also superior, being around 15% greater than on Pt/C. These results indicate that Pt/TiO_2NCs-C has a higher catalytic activity towards EOR than Pt/C, in agreement with previous reports.[38]

In terms of stability, the performance of the Pt/TiO_2NCs-C and Pt/C is shown in Figure 4c. This Figure shows the maximum current density of the forward scan collected by changing the potential exhaustively by up to 70 consecutive voltammogram cycles from 0.05 to 1.0 V vs RHE. This limited window of potential was chosen to preserve the morphologic characteristics of the materials. Both electrocatalysts exhibited a slight drop in their current density. However, Pt/TiO_2NCs-C maintained higher current densities throughout the experiment. Considering the evaluation of medium-term performance, Pt/TiO_2NCs-C lost about 5% of its maximum current density after the 70th CV cycle, while the traditional Pt/C decreased its performance by 10%. Such a decrease in performance could be attributed to

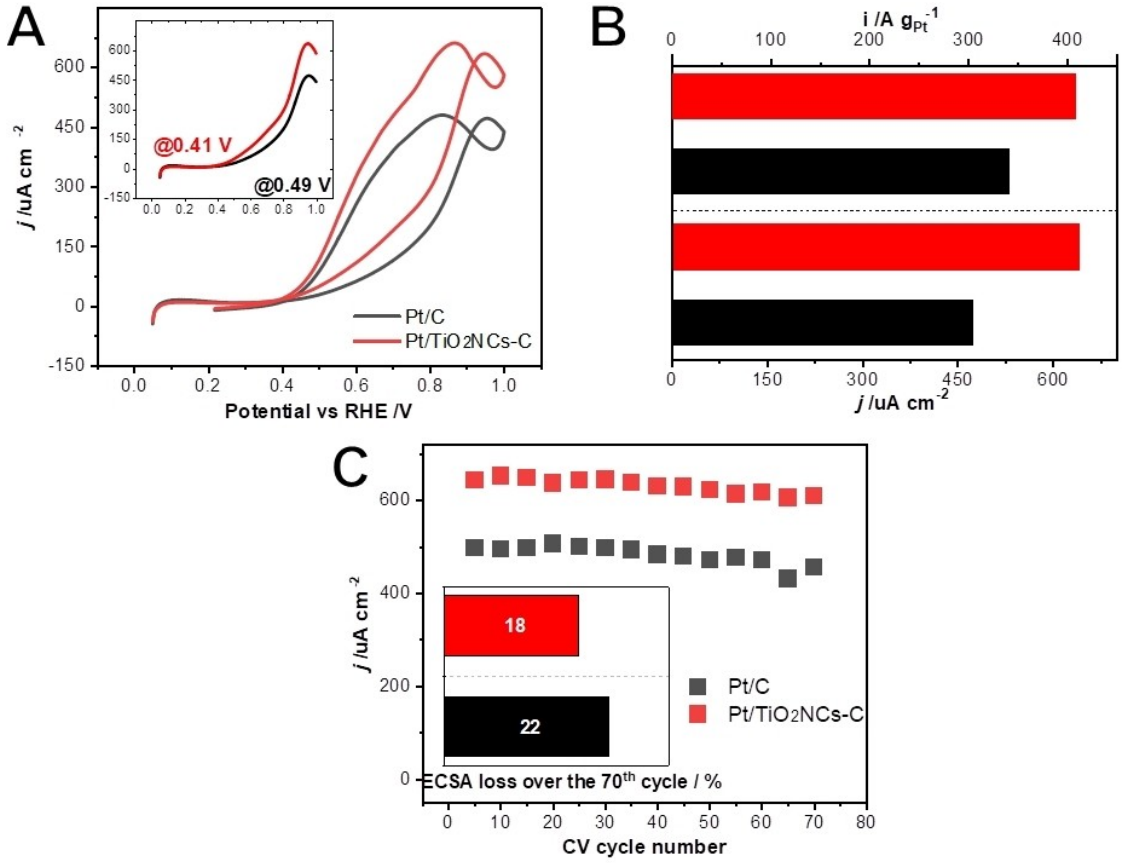

Figure 4. Catalytic activity towards the EOR on Pt/C and Pt/TiO_2NCs-C. (A) CV curves were carried out in 0.5 mol L^{-1} of H_2SO_4 electrolytes containing 1 mol L^{-1} of ethanol at a scan rate of 0.05 V s^{-1} at ambient temperature. Current densities were normalized by Pt mass. (B) maximum CV current density normalized per Pt mass (top panel) and specific area (bottom panel), (C) maximum current densities along 70 voltammetry cycles.

the poisoning effect of the incomplete ethanol fragments such as CO and/or to the loss of Pt active sites. To evaluate the possibility of Pt agglomeration and/or loss of Pt electroactive sites, we monitored the region of hydrogen desorption charge after 70 CV cycles with H_2SO_4 (0.5 mol L^{-1}) as illustrated in Figure 4c inset. In the case of Pt/TiO_2NCs-C, about an 18% decrease in ECSA value was detected after 70 cycles, while for Pt/C, this value corresponded to 22%. In the case of Pt/TiO_2-C, the decrease in ECSA corresponded to 21%. Therefore, these data indicate that Pt/TiO_2NCs-C, in addition to better performances, also displays better stability.[53] The improved medium-term stability of the material containing TiO_2NCs may be related to the more poisoning-resistant characteristics and/or to prevent the Pt electroactive sites loss as well as the fact that Vulcan Carbon is susceptible to support corrosion, thus leading to the detachment and agglomerating of Pt NPs (the formation of oxidizing species such PtO and PtOH can also contribute to the carbon corrosion).[28] In this case, we believe that the utilization of TiO_2 and the strong metal-support interaction between Pt NPs and the TiO_2NCs support can contribute to mitigating this effect.

Figure S5 shows the activity towards methanol, ethylene glycol, and glycerol electrooxidation reaction catalyzed by Pt/C and Pt/TiO_2NCs-C, respectively. For all three alcohols, Pt/TiO_2NCs-C exhibited higher current densities than Pt/C. The maximum current densities for Pt/TiO_2NCs-C were 2.05, 1.26, and 1.47 folds higher for the electrooxidation of methanol, ethylene glycol, and glycerol, respectively. Besides, the onset potential for the Pt/TiO_2NCs-C electrocatalyst was lowered compared with those of Pt/C.

Interestingly, we found that the TiO_2NCs can also be added to commercial electrocatalysts to improve their performances. We could further improve the electrocatalytic activity of the commercial PtSn/C by adding 10 wt.% of TiO_2NCs simply through mixing. The evaluation EOR towards PtSn/C and PtSn/C + TiO_2NCs 10% is shown in Figure S6. PtSn-based materials are known as the best catalysts for the EOR.[54,55] The maximum current densities described in Figure S6A were obtained during 70 CV cycles. Along with the test, higher current density values were obtained when TiO_2NCs were added. From the first CV cycle, it is possible to verify that the current density was about 565 A g_{Pt}^{-1} and 550 A g_{Pt}^{-1} for PtSn/C + TiO_2NCs 10% and PtSn/C, respectively. Over the CV tests, the activity difference has begun to increase and after 70 CV cycles, the current density loss for PtSn/C (~100 A g_{Pt}^{-1}) doubled as compared to PtSn/C + TiO_2NCs 10% material (~50 A g_{Pt}^{-1}). The relative activity loss, given in percentage, is shown in Figure S6B–C. The current density loss over the 70th CV cycle for PtSn/C + TiO_2NCs 10% was approximately 10%, while for PtSn/C was about 18%. This indicates that the addition of a small amount of TiO_2NCs to Pt/C and PtSn/C would help to preserve oxidative characteristics even with the extensive potential cycling. Another potential explanation for the EOR enhancement derivates from a more complete ethanol electrooxidation to CO_2. This could be understood by the fact that the hydroxyl species from TiO_2NCs in Pt/TiO_2NCs-C and PtSn/C + TiO_2NCs 10% electrocatalysts improve the conversion of CO into CO_2 through the bifunctional mechanism. Similar results were also reported by Colpan et al[56] by evaluating PtRu/C-TiO_2 catalyst, in which Ru assumes the same role as Sn co-catalyst.

Finally, we employed the developed electrocatalysts as applied anodes for a PEMFC device, testing their electrical performance by polarization and power density curves (V *vs* *j* – normalized per electrode area) for the electrocatalytic activity of CO-contaminated H_2 in operational fuel cell conditions (Figure 5). Here, the Pt/TiO_2NCs-C and Pt/C were compared. The PEMFC anode devices were both fed with an H_2/CO mixture (100 ppm CO, Figure 5a) and pure hydrogen (Figure 5b, inset) at practical operating temperature (80 °C). Oxygen was chosen as a cathodic oxidizing gas, catalyzed by commercial Pt/C. PEMFC containing both the Pt/C and Pt/TiO_2NCs-C anodes presented similar Open Circuit Voltages (OCV), at approximately

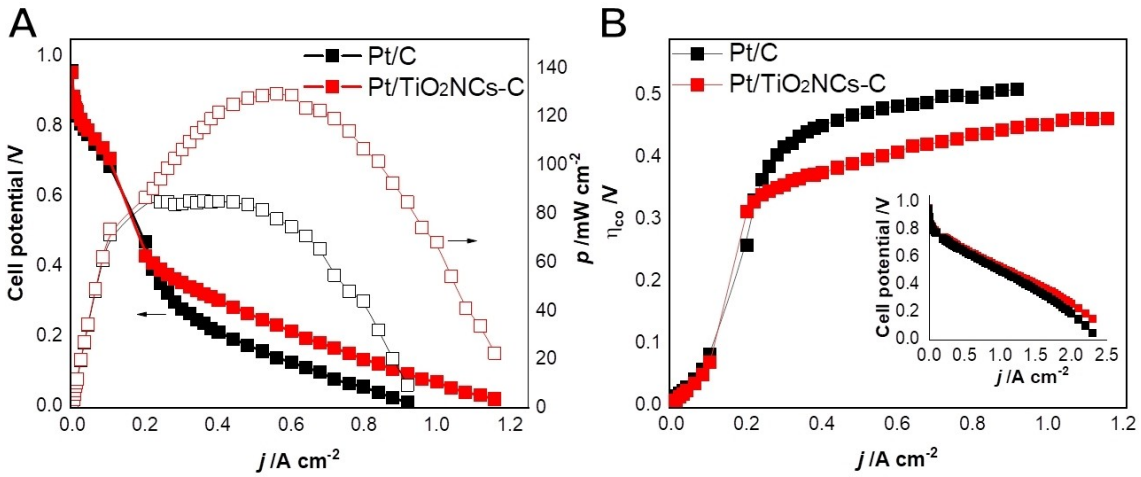

Figure 5. Single-cell performance plots for Pt/C and Pt/TiO_2NCs-C electrodes. (A) polarization (solid squares) and power density curves (open squares) of PEMFC fueled with H_2-CO (100 ppm). (B) CO overpotential (η_{co}) as a function of drained current and polarization curves with PEMFC anode fueled with pure H_2 in the graphical inset. Both current densities were normalized per PEMFC electrode area.

0.96 V in H_2/O_2 and $H_2/CO/O_2$ configurations. Furthermore, both materials exhibited similar electrical performances with H_2/O_2. As can be observed in the graphical inset, the maximum current densities measured were about 2.3 A cm^{-2}. As expected, such electrical performances decreased when both anodes were supplied with CO-contaminated hydrogen. More importantly, higher performances were achieved for the Pt/TiO_2NCs-C material. The maximum current density drained of Pt/TiO_2NCs-C was about 1.2 A cm^{-2}, while for Pt/C catalyst this value was only 0.9 A cm^{-2} in $H_2/CO/O_2$ fueled tests. Power density curves (expressed by open squares) were calculated based on polarization curves. The maximum power density reached by Pt/TiO_2NCs-C was 130 mW cm^{-2}. This value is 65% higher than the obtained by Pt/C electrocatalyst. It is noteworthy that both materials have the same Pt mass, hence both PEMFC electrodes are equally loaded in terms of the active metal. Then, the increased electrical performance of Pt/TiO_2NCs-C was related to the presence of TiO_2 nanocubes, which enables the oxidation of CO at lower overpotentials in comparison to the Pt/C.

This tolerance to CO poisoning effect on Pt/TiO_2NCs-C catalyst is further evidenced by comparing the single-cell anode overpotential (η_{CO}) as a function of the measured PEMFC current density. Figure 5b demonstrate, as also observed in Figure 3, that CO is oxidized at lower potential values on Pt/TiO_2NCs-C relative Pt/C. At the PEMFC operating temperature conditions, the gap of potential between Pt/TiO_2NCs-C and Pt/C observed in Figure 5b was at about 0.08V, in agreement with CO stripping tests performed at ambient temperature, which further suggests that the catalytic activity difference is primarily structural/compositional.

Conclusions

We reported on the development of hybrid support for the deposition of Pt NPs comprising of TiO_2 nanocubes and carbon (TiO_2NCs-C). Pt/TiO_2NCs-C electrocatalyst was synthesized and investigated towards the electrooxidation of carbon monoxide and alcohol. The performances were compared relative to the use of commercial TiO_2 as well as the use of only carbon (Pt/TiO_2-C and Pt/C). In these materials, the Pt NPs size and distribution over the supports were similar. However, the surface characteristics were remarkably changed in terms of Pt-TiO_2 interaction. Electrochemical investigation of the CO-stripping clearly showed that CO interacts differently with Pt/C, Pt/TiO_2NCs-C, and Pt/TiO_2-C. In particular, CO oxidation on Pt/TiO_2NCs-C was greatly facilitated in lower onset potentials, which was due to the strong metal-support interaction and/or bifunctional mechanism provided by Pt nanoparticles and TiO_2 nanocubes. The electrocatalytic activity and the stability of Pt/TiO_2NCs-C for ethanol electrooxidation were also improved relative to the other materials. The medium-term evaluation showed that the loss of Pt active sites phenomena could be suppressed considering the ECSA examination in Pt/TiO_2NCs-C. It is important to note that this system may be further optimized by controlling the size and nature of the Pt species at the TiO_2 surface (NPs, clusters, and single atoms), the shape of Pt NPs (deposition of cubes, octahedra, or shapes enabling the exposure of high index facets), the size of the TiO_2 nanocubes, and the amount of surface defects such as oxygen vacancies. We believe our data indicates that the shape control over the support material can play an important role and can be applied as a promising approach to optimizing electrocatalytic activity and stability in the design of PEMFC and DAFC anodes.

Acknowledgements

The authors thank FAPESP (Proc. number 2017/15469-5, 2015/11452-5, 2016/00819-8, 2016/17866-9, 2014/09087-4, 2017/11937-4 (FAPESP/Shell CINE), and 2015/26308-7), CNPq, and CAPES for the financial support. P.H.C.C. and J.Q. thank the Jane and Aatos Erkko Foundation and the University of Helsinki for the financial support. The use of TEM facilities (JEOL JEM-2100F) of LNNano-CNPEM is acknowledged.

Conflict of Interest

The authors declare no conflict of interest.

Keywords: fuel cells · Pt nanoparticles · TiO_2 nanocubes · electrocatalysis · CO tolerance

[1] E. Antolini, *J. Power Sources* **2007**, *170*, 1–12.
[2] M. A. F. Akhairi, S. K. Kamarudin, *Int. J. Hydrogen Energy* **2016**, *41*, 4214–4228.
[3] S. G. da Silva, M. H. M. T. Assumpção, R. F. B. de Souza, G. S. Buzzo, E. V. Spinacé, A. O. Neto, J. C. M. Silva, *Electrocatalysis* **2014**, *5*, 438–444.
[4] E. E. Switzer, T. S. Olson, A. K. Datye, P. Atanassov, M. R. Hibbs, C. J. Cornelius, *Electrochim. Acta* **2009**, *54*, 989–995.
[5] H. Gao, S. Liao, Z. Liang, H. Liang, F. Luo, *J. Power Sources* **2011**, *196*, 6138–6143.
[6] J. P. I. De Souza, S. L. Queiroz, K. Bergamaski, E. R. Gonzalez, F. C. Nart, *J. Phys. Chem. B* **2002**, *106*, 9825–9830.
[7] A. Kumar, K. Kumar, V. Krishnan, *Mater. Lett.* **2019**, *245*, 45–48.
[8] J. Han, L. Yang, L. Yang, W. Jiang, X. Luo, S. Luo, *Int. J. Hydrogen Energy* **2018**, *43*, 7338–7346.
[9] O. Schmidt, A. Gambhir, I. Staffell, A. Hawkes, J. Nelson, S. Few, *Int. J. Hydrogen Energy* **2017**, *42*, 30470–30492.
[10] C. Busó-Rogero, S. Brimaud, J. Solla-Gullon, F. J. Vidal-Iglesias, E. Herrero, R. J. Behm, J. M. Feliu, *J. Electroanal. Chem.* **2016**, *763*, 116–124.
[11] J. Bai, D. Liu, J. Yang, Y. Chen, *ChemSusChem* **2019**, *12*, 2117–2132.
[12] P. Chandran, A. Ghosh, S. Ramaprabhu, *Sci. Rep.* **2018**, *8*, 1–11.
[13] A. Kongkanand, N. P. Subramanian, Y. Yu, Z. Liu, H. Igarashi, D. A. Muller, *ACS Catal.* **2016**, *6*, 1578–1583.
[14] S. Shahgaldi, J. Hamelin, *Carbon* **2015**, *94*, 705–728.
[15] J. Xi, J. Wang, L. Yu, X. Qiu, L. Chen, *Chem. Commun.* **2007**, 1656–1658.
[16] W. Wang, W. Wang, S. Chen, *Int. J. Hydrogen Energy* **2016**, *41*, 20680–20692.
[17] V. Grozovski, V. Climent, E. Herrero, J. M. Feliu, *J. Electroanal. Chem.* **2011**, *662*, 43–51.
[18] C. Lamy, S. Rousseau, E. M. Belgsir, C. Coutanceau, J. M. Léger, *Electrochim. Acta* **2004**, *49*, 3901–3908.
[19] L. Jiang, L. Colmenares, Z. Jusys, G. Q. Sun, R. J. Behm, *Electrochim. Acta* **2007**, *53*, 377–389.
[20] A. Kowal, M. Li, M. Shao, K. Sasaki, M. B. Vukmirovic, J. Zhang, N. S. Marinkovic, P. Liu, A. I. Frenkel, R. R. Adzic, *Nat. Mater.* **2009**, *8*, 325–330.
[21] G. García, N. Tsiouvaras, E. Pastor, M. A. Peña, J. L. G. Fierro, M. V. Martínez-Huerta, *Int. J. Hydrogen Energy* **2012**, *37*, 7131–7140.
[22] R. M. Antoniassi, J. C. M. Silva, A. Oliveira Neto, E. V. Spinacé, *Appl. Catal. B* **2017**, *218*, 91–100.

[23] J. R. Barbosa, M. N. Leon, C. M. Fernandes, R. M. Antoniassi, O. C. Alves, E. A. Ponzio, J. C. M. Silva, *Appl. Catal. B* **2020**, *264*, 118458.
[24] N. Coustel, B. Coq, V. Brotons, P. S. Kumbhar, R. Dutartre, P. Geneste, J. M. Planeix, P. Bernier, P. M. Ajayan, *J. Am. Chem. Soc.* **1994**, *116*, 7935–7936.
[25] N. S. Marinkovic, M. Li, R. R. Adzic, *Top. Curr. Chem.* **2019**, DOI 10.1007/s41061-019-0236–5.
[26] Y. Ma, B. Cui, L. He, K. Tian, Z. Zhang, M. Wang, *J. Electroanal. Chem.* **2019**, *850*, 113435.
[27] Z. Siroma, K. Ishii, K. Yasuda, Y. Miyazaki, M. Inaba, A. Tasaka, *Electrochem. Commun.* **2005**, *7*, 1153–1156.
[28] W. Li, A. M. Lane, *Electrochem. Commun.* **2009**, *11*, 1187–1190.
[29] P. Mohanta, F. Regnet, L. Jörissen, *Materials (Basel).* **2018**, *11*, 907.
[30] Y. Shao, G. Yin, Y. Gao, P. Shi, *J. Electrochem. Soc.* **2006**, *153*, A1093.
[31] T. Ioroi, Z. Siroma, S. Yamazaki, K. Yasuda, *Adv. Energy Mater.* **2019**, *9*, 1801284.
[32] C. J. Pan, M. C. Tsai, W. N. Su, J. Rick, N. G. Akalework, A. K. Agegnehu, S. Y. Cheng, B. J. Hwang, *J. Inst. Chem.* **2017**, *74*, 154–186.
[33] K. Singh, E. B. Tetteh, H.-Y. Lee, T.-H. Kang, J.-S. Yu, *ACS Catal.* **2019**, *9*, 8622–8645.
[34] E. Antolini, *Appl. Catal. B* **2009**, *88*, 1–24.
[35] M. N. Groves, A. S. W. Chan, C. Malardier-Jugroot, M. Jugroot, *Chem. Phys. Lett.* **2009**, *481*, 214–219.
[36] J. Wang, Y. Chen, Y. Zhang, M. I. Ionescu, R. Li, X. Sun, S. Ye, S. Knights, *J. Mater. Chem.* **2011**, *21*, 18195–18198.
[37] T. Maiyalagan, *Appl. Catal. B* **2008**, *80*, 286–295.
[38] Q. Lv, M. Yin, X. Zhao, C. Li, C. Liu, W. Xing, *J. Power Sources* **2012**, *218*, 93–99.
[39] D. Zhang, C. Zhang, Y. Chen, Q. Wang, L. Bian, J. Miao, *Electrochim. Acta* **2014**, *139*, 42–47.
[40] Z. Cui, L. Feng, C. Liu, W. Xing, *J. Power Sources* **2011**, *196*, 2621–2626.
[41] F. V. E. dos Reis, V. S. Antonin, P. Hammer, M. C. Santos, P. H. C. Camargo, *J. Catal.* **2015**, *326*, 100–106.
[42] X. Yang, Y. Yang, H. Hou, Y. Zhang, L. Fang, J. Chen, X. Ji, *J. Phys. Chem. C* **2015**, *119*, 3923–3930.
[43] R. M. Antoniassi, A. Oliveira Neto, M. Linardi, E. V. Spinacé, *Int. J. Hydrogen Energy* **2013**, *38*, 12069–12077.
[44] X. H. Yang, Z. Li, C. Sun, H. G. Yang, C. Li, *Chem. Mater.* **2011**, *23*, 3486–3494.
[45] Y. Ji, Y. il Cho, Y. Jeon, C. Lee, D. Park, Y. G. Shul, *Appl. Catal. B* **2017**, *204*, 421–429.
[46] A. Lewera, L. Timperman, A. Roguska, N. Alonso-Vante, *J. Phys. Chem. C* **2011**, *115*, 20153–20159.
[47] S. Yoon, K. Oh, F. Liu, J. H. Seo, G. A. Somorjai, J. H. Lee, K. An, *ACS Catal.* **2018**, *8*, 5391–5398.
[48] Y. Chen, J. Shi, S. Chen, *J. Phys. Chem. C* **2015**, *119*, 7138–7145.
[49] Y. H. Qin, Y. Li, R. L. Lv, T. L. Wang, W. G. Wang, C. W. Wang, *J. Power Sources* **2015**, *278*, 639–644.
[50] W. Vogel, L. Timperman, N. Alonso-Vante, *Appl. Catal. A* **2010**, *377*, 167–173.
[51] B. J. Hsieh, M. C. Tsai, C. J. Pan, W. N. Su, J. Rick, H. L. Chou, J. F. Lee, B. J. Hwang, *Electrochim. Acta* **2017**, *224*, 452–459.
[52] Z. Z. Jiang, Z. B. Wang, Y. Y. Chu, D. M. Gu, G. P. Yin, *Energy Environ. Sci.* **2011**, *4*, 728–735.
[53] D. Banham, S. Ye, *ACS Energy Lett.* **2017**, *2*, 629–638.
[54] F. L. S. Purgato, S. Pronier, P. Olivi, A. R. De Andrade, J. M. Léger, G. Tremiliosi-Filho, K. B. Kokoh, *J. Power Sources* **2012**, *198*, 95–99.
[55] E. Lee, A. Murthy, A. Manthiram, *Electrochim. Acta* **2011**, *56*, 1611–1618.
[56] M. Ercelik, A. Ozden, E. Seker, C. O. Colpan, *Int. J. Hydrogen Energy* **2017**, *42*, 21518–21529.

Manuscript received: December 28, 2020
Revised manuscript received: January 13, 2021
Accepted manuscript online: January 18, 2021
Version of record online: February 18, 2021